Proceedings of the
International Conference on Mechanical Engineering 2009
(ICME2009) 26- 28 December 2009, Dhaka, Bangladesh

ICME09-FM-09

A COMPUTATIONAL STUDY OF TRANSONIC MOIST AIR FLOW AROUND A SYMMETRIC DISK BUTTERFLY VALVE

A. B. M. Toufique Hasan[1], Mohammad Mamun[2], Shigeru Matsuo[3] and Toshiaki Setoguchi[4]

[1] Graduate School of Science and Engineering, Saga University, Saga, Japan
[2] Department of Mechanical Engineering, Bangladesh University of Engineering and Technology, Dhaka , Bangladesh
[3]Department of Mechanical Engineering, Saga University, Saga, Japan
[4] Institute of Ocean Energy, Saga University, Saga, Japan

ABSTRACT

Transonic flow around a symmetric disk butterfly valve is associated with the appearance of shock waves standing on valve surfaces. In this case, the interaction between shock wave and boundary layer becomes complex and thus generates the flow induced aerodynamic instability. In the transonic or supersonic flow where vapour is contained in the main flow, the rapid expansion of the flow may give rise to non-equilibrium condensation. In the present study, the effect of non-equilibrium condensation of moist air on the shock induced flow field oscillation around a butterfly valve was investigated numerically. The results showed that in case with non-equilibrium condensation, the flow field aerodynamic instabilities such as root mean square of pressure oscillation and shock induced oscillation frequency are reduced significantly compared with those without the non-equilibrium condensation. Moreover, the total pressure loss increases and the vortex shedding frequency is reduced with non-equilibrium condensation.

Keywords: Transonic Flow, Shock Induced Oscillation, Moist Air.

1. INTRODUCTION

Shock-boundary layer interaction (SBLI) is often observed in many transonic internal aeronautical applications such as turbine cascades, compressor blades, butterfly valves, fans, nozzles, diffusers and so on. Shock induced oscillations (SIO), aerodynamic instabilities (buffet), high cycle fatigue failure (HCF), nonsynchronous vibration (NSV), flutter, aeroacoustic noise and vibration and so on are the detrimental consequences of this unsteady interaction [1-2]. In transonic or supersonic flow where water vapour is contained in the main flow, rapid expansion may give rise to non-equilibrium condensation [3-5]. In this case, the degree of supersaturation $S = p_v/p_{s,\infty}(T)$ (where p_v is the water vapour pressure and $p_{s,\infty}(T)$ is the saturation pressure of water vapour at a given temperature T) may reach much above one ($S >> 1$) without condensation because the liquid droplets do not reach the critical size for growth and collapse back to water vapour. At the critical state, known as supersaturation state, the liquid droplets reach the critical size. A significant nucleation of water droplets is suddenly initiated by spontaneous fluctuations in water vapour itself, known as homogenous nucleation [**3**]. Further, the condensation of the vapour takes place on these nuclei, known as droplet growth. This condensation process releases thermal energy to the surrounding gaseous medium andconsiderably modifies their thermo-fluid behaviors.

Butterfly valve disks behave similarly to airfoils in that the angle of attack influences the flow field characteristics [6]. However, under certain combinations of valve disk opening angle and pressure difference across the valve, compressible flow effects can significantly alter the performance characteristics and flowfield of a butterfly valve. At these conditions, regions of transonic and supersonic flow can develop in the vicinity of the valve disk and downstream of it. Recently, butterfly valve performance coefficients in compressible flow field were predicted using computational fluid dynamics (CFD) [6-7]. However, in transonic or supersonic flow field, expansion of vapor/carrier gas mixture (moist air) or steam is often so rapid that the flow field gives rise to non-equilibrium condensation process. Till now, there is no investigation concerning the working medium as a moist air in the flow field around a butterfly valve.

In the present study, the effect of moist air with the occurrences of non-equilibrium condensation on transonic internal flow around a symmetric disk butterfly valve is investigated numerically. The computational results are also validated with experiments. Furthermore, various aerodynamic aspects for the case of moist air are

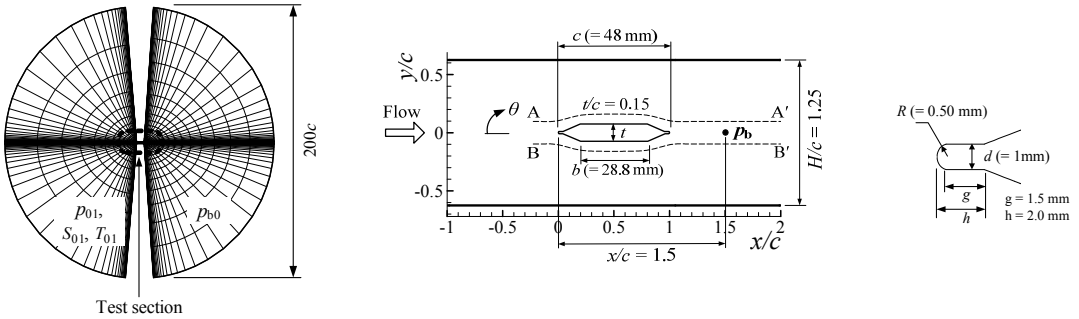

(a) Computational domain (b) Details of test section (c) Valve edge

Fig 1. Computational domain, test section and valve edge geometry

discussed and compared with results of dry air.

2. NUMERICAL METHODS

Governing equations of the present flow field are unsteady compressible Navier-Stokes equations written in two-dimensional coordinate system. To link the heat supply by condensation process with flow, a rate equation of liquid-phase production [8] is coupled. As a turbulence model, a modified two-equation *k*-*R* model [9-10] was used in the present computation where *k* is the turbulent kinetic energy and *R* being the undamped eddy viscosity.

These equations were discretized by the finite difference technique. A third order TVD (total variation diminishing) finite difference scheme with MUSCL [11] was employed to discretize the spatial derivative, and a second order central difference scheme for viscous terms, and a second order fractional step was used for time integration. For simplicity of the computation, assumptions are as follows; no velocity slip and no temperature difference between condensate particles and gas medium, and the effect of condensate particles on pressure is negligible.

Figure 1 shows the computational domain of the flow field, details of test section and valve edge geometry. Chord length c and the thickness of the butterfly valve t are 48 mm and 7.2 mm (t/c = 0.15), respectively. Valve leading and trailing edges are rounded with radius of 0.5 mm. The height of the test section H is 60 mm (H/c = 1.25). Computational domain is discretized by structured mesh. The mesh size is 351×101. The origin of (x, y) coordinate is located at leading edge of the valve. Aerodynamic and condensate properties are measured along lines A-A′ and B-B′ which are vertically 0.075c apart from the valve upper surface and lower surface, respectively.

Working gas used in the present study is moist air which is assumed to be thermally and calorically perfect. Inlet Mach number upstream of the valve is 0.6 and Reynolds number based on valve chord length is 5.4×10^5. The pressure ratio p_{b0}/p_{01} (p_{b0} : total back pressure, p_{01} : reservoir total pressure) was kept at 0.739 [12]. Initial degrees of supersaturation S_{01} are 0 for dry air and 0.6 for moist air. Total temperature T_{01} and total pressure p_{01} in the reservoir are 298.15 K and 101.3 kPa, respectively.

Inlet boundary was fixed, and exit boundary was constrained with free boundary condition. Non-slip and adiabatic wall conditions were applied at the solid boundary. The pressure at the wall was obtained from zero normal pressure gradient on the body surface. Condensate mass fraction g was set to zero on the solid wall.

3. RESULTS AND DISCUSSION

Figures 2(a) and 2(b) show instantaneous schlieren photographs around a symmetric disk butterfly valve in cases without and with non-equilibrium condensation by experiments, respectively (θ = 0° and p_b/p_{01} = 0.650). Figures 3 show instantaneous schlieren photographs around a symmetric disk butterfly valve obtained by experiments for θ = 3.2°. Results for S_{01} = 0.17 (Figs. 2(a) and 3(a)) are shown in these figures. In this case, the degree of supersaturation is so small that the air can be considered to be almost dry [5]. In case with non-equilibrium condensation (Figs. 2(b) and 3(b)), it seems that the configuration of the shock wave changes largely and its strength becomes weaker compared to those in Figs. 2(a) and 3(a). However, in case of S_{01}= 0.6, the shock wave moves further upstream to that of dry air for θ = 3.2°. Figures 4 and 5 show computer generated schlieren pictures (density gradient) corresponding to each figure in Figs. 2 and 3, respectively. As seen from these figures, the flow structures obtained by simulation are similar to experimental results. However, small difference in shock structure in between experiment and simulation is due to presence of three-dimensional phenomena in the actual flow field.

Figure 6 shows the distributions of static pressure p/p_{01}, nucleation rate I and condensate mass fraction g along the lines A-A′ and B-B′ during one cycle of shock oscillation T_s for θ = 0°. T_s is the time period of one cycle of shock induced oscillation measured at the peak position of RMS value of pressure oscillation (will be discussed latter). In case of S_{01} = 0, shock waves along line A-A′ are observed to develop from $x/c \approx 0.5$ and travel toward the leading edge during the cycle. Along line B-B′, shock waves are moving from leading to trailing edge. Thus, shock waves are oscillating alternatively in between the upper and lower passages during the cycle. In case of S_{01} = 0.6, the maximum degree of expansion in the flow field is reduced and thus strength of shock wave becomes weak compared to the case of S_{01} = 0. Furthermore, the distribution of p/p_{01} indicates that the strength of shock wave gradually decreases when shock wave is moving towards the leading edge of the valve in both the cases. With the

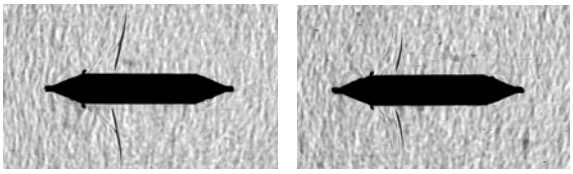

(a) S_{01} = 0.17 (b) S_{01} = 0.6

Fig 2. Schlieren photographs (θ = 0°, p_b/p_{01} = 0.650)

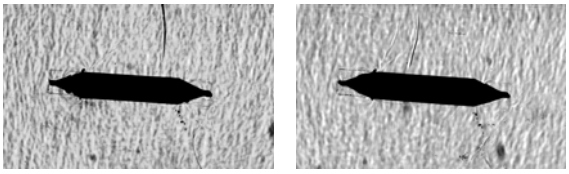

(a) S_{01} = 0.17 (b) S_{01} = 0.6

Fig 3. Schlieren photographs (θ = 3.2°, p_b/p_{01} = 0.650)

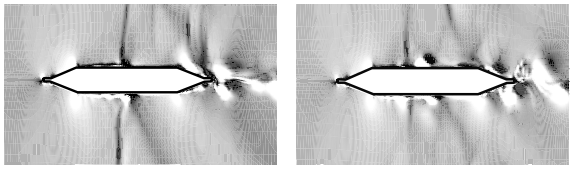

(a) S_{01} = 0.17 (b) S_{01} = 0.6

Fig 4. Computer numerical Schlieren (θ = 0°, p_b/p_{01} = 0.650)

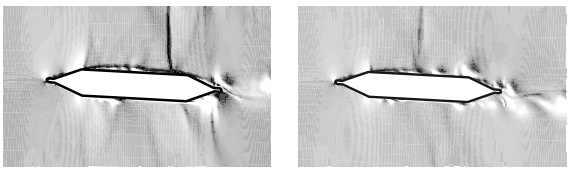

(a) S_{01} = 0.17 (b) S_{01} = 0.6

Fig 5. Computer numerical Schlieren (θ = 3.2°, p_b/p_{01} = 0.650)

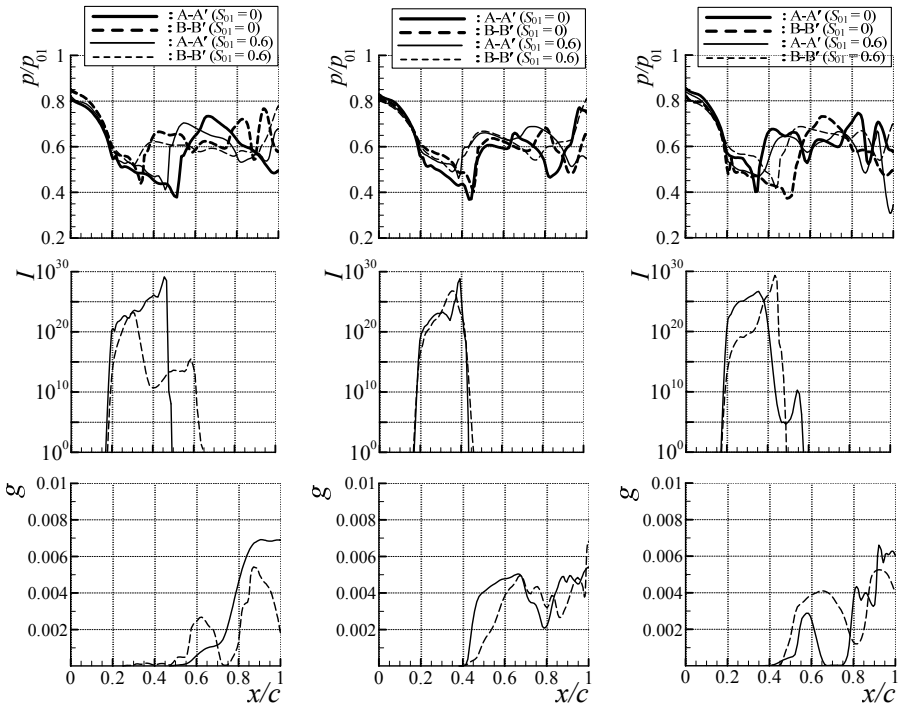

(a) t = 0.333 T_s (ms) (b) t = 0.667 T_s (ms) (c) t = 1.000 T_s (ms)

Fig 6. Distributions of static pressure (p/p_{01}), nucleation rate (I) and condensate mass fraction (g) around a valve (θ = 0°, p_{b0}/p_{01} = 0.739)

occurrence of non-equilibrium condensation (S_{01}= 0.6), a nucleation zone is observed to develop in the region close to rapid flow expansion at $x/c \approx 0.2$. Nucleation rate I reaches the peak value and then decreases with sharp gradient where static pressure falls to a minimum. Condensate mass fraction g begins to increase approximately from the position where nucleation rate decreases sharply. At upper region (along line A-A′), g starts to increase at x/c = 0.48, 0.40 and 0.35 for t = $0.333T_s$, $0.667T_s$ and $1.000T_s$, respectively. It is found from the above results that in upper region, positions where g begins to increase move towards the leading edge of the valve during the cycle. For lower region (along line B-B′), the positions where g begins to develop move towards the trailing edge of the valve during the cycle. Thus, condensate properties I and g generate alternatively between the upper and lower regions around the valve. After the initial development, g varies unevenly further downstream. The maximum of g values are about 0.006 along the lines A-A′ and B-B′. The reduction of shock strength is considered to be due to reduction of Mach number upstream of the shock by the generation of liquid droplets in case of moist air.

Figure 7 shows the distributions of static pressure p/p_{01}, nucleation rate I and condensate mass fraction g along the lines A-A′ and B-B′ during one cycle of shock oscillation T_s for θ = 3.2°. At θ = 3.2°, stronger shock wave is generated around the valve upper surface compared to θ = 0° (Fig. 6) in the range of $x/c \approx 0.5 \sim 1.0$ for S_{01}= 0. In the lower surface, the shock wave is weaker

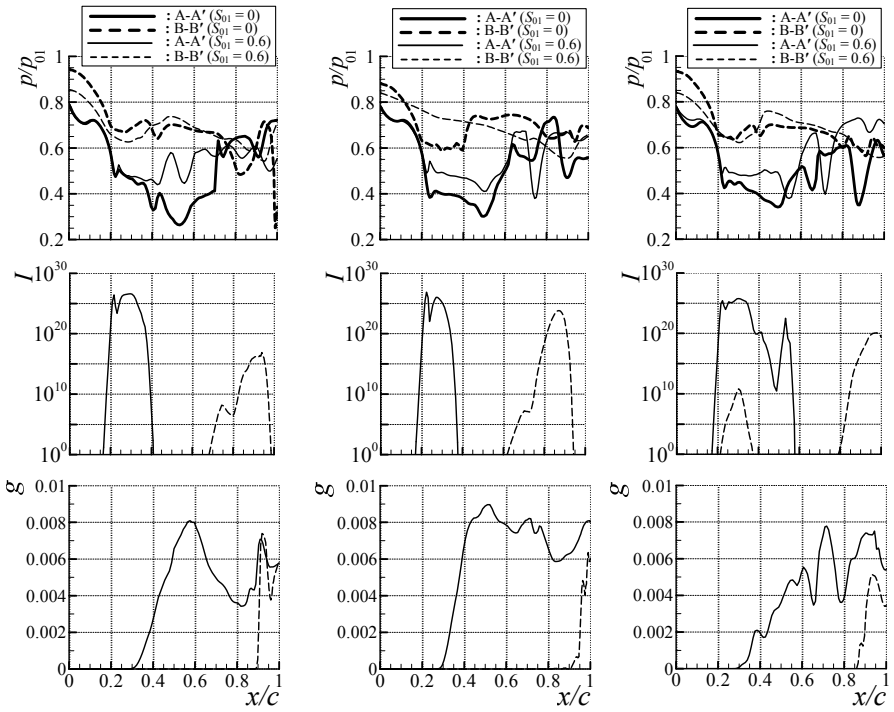

(a) t = 0.333 T_s (ms) (b) t = 0.667 T_s (ms) (c) t = 1.000 T_s (ms)

Fig 7. Distributions of static pressure (p/p_{01}), nucleation rate (I) and condensate mass fraction (g) around a valve (θ = 3.2°, p_{b0}/p_{01} = 0.739)

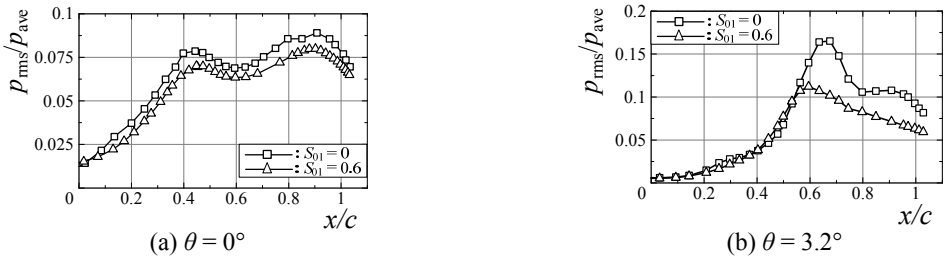

(a) θ = 0° (b) θ = 3.2°

Fig 8. Distribution of RMS value of pressure oscillation around the valve (p_{b0}/p_{01} = 0.739)

than the upper one. In case of the occurrence of non-equilibrium condensation (S_{01} = 0.6), along line A-A′, a nucleation zone is developed around the valve leading edge. Then a sharp gradient in decrease of nucleation rate is observed at about x/c = 0.25. This initiates the development of condensate mass fraction from this position ($x/c \approx 0.25$). In lower region along line B-B′, the reduction of degree of flow expansion causes in decrease of peak nucleation rate compared to upper region. g begins to increase from $x/c \approx 0.85$ along this line. The maximum of g values are about 0.008 and 0.006 along the lines A-A′ and B-B′, respectively. Furthermore, generation of liquid droplets also reduces the shock strength in both upper and lower regions at this angle of attack (θ = 3.2°).

Flow field aerodynamic instability around the valve due to shock induced oscillation can conveniently be explained by the distribution of root mean square (RMS) value of pressure oscillation. Figure 8 shows the distribution of RMS value of pressure oscillation p_{rms}/p_{ave} (p_{rms}: RMS of pressure oscillation; p_{ave}: average of pressure oscillation) around upper passage of the test section for θ = 0° and 3.2° in cases without and with non-equilibrium condensation. At θ = 0° (Fig. 8(a)), two peaks are observed in both the cases of S_{01} = 0 and S_{01} = 0.6. However, the second one is more dominating than the first and located at about x/c = 0.9. In all axial locations, the RMS values are smaller in case of S_{01} = 0.6 to those of S_{01} = 0. The peak p_{rms}/p_{ave} values are 0.09 and 0.08 for S_{01} = 0 and S_{01} = 0.6, respectively. For θ = 3.2° (Fig. 8(b)), the RMS values are comparable up to x/c = 0.55 in both the cases of S_{01} = 0 and 0.6. After that, the RMS values are reduced in case of S_{01} = 0.6. The peak RMS values are 0.17 and 0.11 for S_{01} = 0 and S_{01} = 0.6, respectively. However, in case of S_{01} = 0.6, peak RMS position is moved further upstream (x/c = 0.58) to that of S_{01} = 0 (x/c = 0.68).

Dominant frequencies of shock induced oscillation measures at the peak position of RMS value of pressure oscillation (Fig. 8) are shown in Table 1. For all angles of attack, the frequencies are reduced significantly with the occurrences of non-equilibrium condensation compared with the case of no condensation. Reduction of dominant frequency is considered to be due to the decrease of turbulent fluctuation energy by the relaxation process of condensation and evaporation of vapour molecules on

Table 1: Dominant frequency (kHz) of shock induced oscillation at peak RMS position of pressure oscillation

S_{01} \ θ	0°	3.2°
0	1.26	1.20
0.6	0.51	0.50

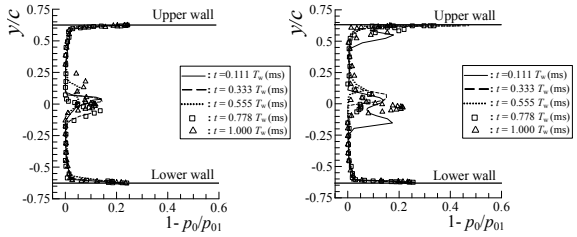

(a) $\theta = 0°$ (b) $\theta = 3.2°$

Fig 9. Total pressure losses during one cycle of flow oscillation (x/c = 1.5, S_{01} = 0)

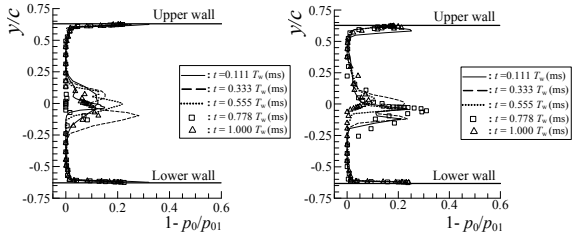

(a) $\theta = 0°$ (b) $\theta = 3.2°$

Fig 10. Total pressure losses during one cycle of flow oscillation (x/c = 1.5, S_{01} = 0.6)

small droplet surfaces, and the interaction of boundary layer with shock wave becomes weak due to reduction of Mach number upstream of the shock wave.

Figure 9 shows distributions of total pressure loss ($1\text{-}p_0/p_{01}$) (p_0: local total pressure) along y-direction at the position of x/c = 1.5 in case without non-equilibrium condensation during one cycle of flow oscillation T_w (S_{01} = 0). T_w is the time period of vortex shedding frequency measured at x/c = 1.5, y/c = 0 (will be discussed latter). For all angles of attack, θ = 0° and 3.2° (Figs. 9(a) and 9(b)), total pressure loss changes largely during one cycle. However, unsteadiness of total pressure losses increases with an increase of angle of attack. The maximums of total pressure loss values for θ = 0° and 3.2° are observed in the range of y/c = - 0.2 ~ 0.2 and - 0.25 ~ 0.25, respectively. For θ = 3.2° (Fig. 9(b)), much variation of total pressure losses are observed in the region close to the upper wall compared with θ = 0°. This is due to the boundary layer separation induced by shock wave at the upper wall. Total pressure losses in case with non-equilibrium condensation along y-direction during one cycle of flow oscillation T_w are shown in Fig. 10 (x/c = 1.5, S_{01} = 0.6). It is found from this figure that values of total pressure loss become larger compared with case of dry air in Fig. 9. Moreover, y-range of occurrence of total pressure losses is increased for angles of attack of 0° and 3.2° compared to Figs. 9(a) and 9(b), respectively. This is considered to be due to the generation of condensate droplets induced by non-equilibrium condensation.

Total pressure losses were integrated from the lower wall to the upper wall at x/c = 1.5 and the time averaged value β is shown for each angles of attack in Table 2.

Table 2: Time average integrated total pressure loss, β (-) (x/c = 1.5, p_{b0}/p_{01} = 0.739)

S_{01} \ θ	0°	3.2°
0	0.035	0.041
0.6	0.044	0.048

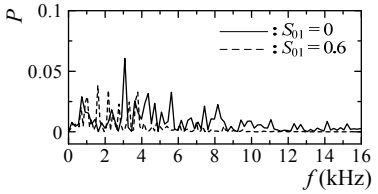

(a) $\theta = 0°$

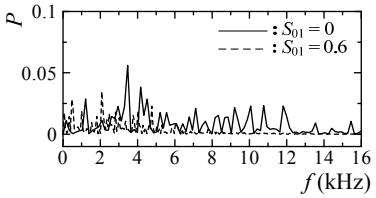

(b) $\theta = 3.2°$

Fig 11. Distributions of power spectrum densities in the wake region at x/c = 1.5

With an increase of angle of attack, β increases in cases without and with non-equilibrium condensation. In case of the occurrence of non-equilibrium condensation, values of β for θ = 0° and 3.2° increase approximately by 25 % and 17 % compared to the case of no condensation, respectively.

Figure 11 shows the distributions of power spectrum densities (PSD) for wake static pressure measured at x/c = 1.5, y/c = 0. For all angles of attack (θ = 0° and 3.2°), it is observed that the vortex shedding frequency contains a frequency band width. However, in case of dry air, the dominant frequencies are 3.08 kHz and 3.48 kHz for θ = 0° and 3.2°, respectively. In case of moist air, the corresponding frequencies are 1.60 kHz and 2.08 kHz. In addition, the frequency band width and peaks of power spectrum densities are reduced in case of moist air to those of dry air.

4. CONCLUSIONS

A computational study has been made to investigate the transonic flow around a symmetric disk butterfly valve at Mach number of 0.6 upstream of the valve for two different angles of attack. Aerodynamic features of the compressible flow field in case of moist air with non-equilibrium condensation were compared with those of dry air numerically and experimentally. The results obtained are summarized as follows: with the occurrence of non-equilibrium condensation, the strength of shock wave was reduced in case of valve with or without angle of attack. In case of valve without angle of attack (θ = 0°), the condensate nuclei and droplets were observed around the valve upper and lower passages alternatively including downstream range. However for θ = 3.2°, condensate properties are observed mainly around the valve upper passage. The shock induced flow field aerodynamic instabilities such as root mean square (RMS) of pressure oscillations and flow oscillation

frequency were reduced significantly with non-equilibrium condensation compared to no condensation case. The peak of RMS value of pressure oscillation was shifted towards the upstream of the valve in case of moist air for valve with angle of attack (θ = 3.2°). However, generation of condensate mass fraction and thus irreversible heat transfer in the flow field increased the total pressure loss in case of moist air. Furthermore, in the wake region, the vortex frequencies as well as peaks of power spectrum densities were reduced in case of moist air to those of dry air.

5. REFERENCES

1. McBean, I., Hourigan, K., Thompson, M. and Liu, F., 2005, "Prediction of Flutter of Turbine Blades in a Transonic Annular Cascade", ASME Journal of Fluids Engineering, 127: 1053-1058.
2. Caruana, D., Mignosi, A., Robitaillé, C. and Corrège, M., 2003, "Separated Flow and Buffeting Control", Flow, Turbulence and Combustion, 71: 221-245.
3. Rusak, Z. and Lee, J.-C., 2000, "Transonic Flow of Moist Air around a Thin Airfoil with Non-Equilibrium and Homogeneous Condensation", Journal of Fluid Mechanics, 403:173-199.
4. Bakhtar, F., Young, J. B., White, A. J. and Simpson, D. A., 2005, "Classical Nucleation Theory and its Application to Condensing Steam Flow Calculations", Proceedings of the Institution of Mechanical Engineers, Part C: Journal of Mechanical Engineering Science, 219:1315-1333.
5. Huang, J. C., Gault, R. I., Benard, E. and Raghunathan, S., 2008, "Effect of Humidity on Transonic Flow", Journal of Aircraft, 45: 2092-2100.
6. Leutwyler, Z., and Dalton, C., 2006, "A Computational Study of Torque and Forces Due to Compressible Flow on a Butterfly Valve in Mid-Stroke Position", ASME Journal of Fluids Engineering, 128: 1074-1082.
7. Leutwyler, Z. and Dalton, C., 2008, "A CFD Study of The Flow Field, Resultant Force, and Aerodynamic Torque an a Symmetric Disk Butterfly Valve in a Compressible Fluid", ASME Journal of Pressure Vessel Technology, 130: 021302-1-021302-10.
8. Sislian, J. P., 1975, *Condensation of Water Vapour with or without a Carrier Gas in a Shock Tube*.UTIAS Report No. 221.
9. Goldberg, U. C., 1994, "Toward a Pointwise Turbulence Model for Wall-Bounded and Free Shear Flows", ASME Journal of Fluids Engineering, 116: 72-76.
10. Heiler, M., 1999, "Instationäre Phänomene in Homogen/Heterogen Kondensierenden Düsen- und Turbinenströmungen", Ph.D. Thesis, Universität Karlsruhe (TH), Germany. (in German)
11. Yee, H. C., 1989, *A Class of High-Resolution Explicit and Implicit Shock Capturing Methods*. NASA TM-89464.
12. Hasan, A. B. M. T., Matsuo, S., Setoguchi, T., Kim, H. D. and Yu, S., 2009, " Control of Transonic Flow with Non-Equilibrium Condensation around a Circular Arc Blade using Bump", International Journal of Turbo and Jet Engines, 26: 33-49.

6. NOMENCLATURE

Symbol	Meaning	Unit
c	Chord length of butterfly valve	(mm)
f	Frequency	(kHz)
g	Condensate mass fraction	(-)
H	Height of test section	(mm)
I	Nucleation rate per unit volume and time	($1/m^3 \cdot s$)
P	Power spectrum density	(-)
P_{01}	Reservoir total pressure	(kPa)
P_b	Back pressure	(kPa)
P_{b0}	Total back pressure	(kPa)
p_v	Water vapour pressure	(Kpa)
$P_{s,\infty}$	Saturation pressure of water vapour	(Kpa)
S	Degree of supersaturation	(-)
t	Time /Thickness	(ms/mm)
T_s	Time period of shock induced oscillation	(ms)
T_w	Time period of wake frequency	(ms)
T_{01}	Reservoir total temperature	(K)
x, y	Cartesian coordinates	(mm)
β	Integrated total pressure loss	(-)
θ	Angle of attack	(°)
0	Local stagnation state	(-)
01	Reservoir state	(-)

7. MAILING ADDRESS

A. B. M. Toufique Hasan
Graduate School of Science and Engineering
Saga University, 1 Honjo-machi,
Saga 840-8502, Japan
Phone: +81 (0)952 28 8606,
FAX: +81 (0)952 28 8587